Lack of Correlation of Hypoxic Cell Fraction and Angiogenesis with Glucose Metabolic Rate in Non–Small Cell Lung Cancer Assessed by ^{18}F-Fluoromisonidazole and ^{18}F-FDG PET

Martin H. Cherk[1], Serene S. Foo[2], Aurora M.T. Poon[1], Simon R. Knight[3], Carmel Murone[2], Anthony T. Papenfuss[4], John I. Sachinidis[1], Timothy H.C. Saunder[1], Graeme J. O'Keefe[1], and Andrew M. Scott[1,2,5]

[1]Centre for PET, Austin Hospital, Heidelberg, Victoria, Australia; [2]Ludwig Institute for Cancer Research, Austin Hospital, Heidelberg, Victoria, Australia; [3]Department of Thoracic Surgery, Austin Hospital, Heidelberg, Victoria, Australia; [4]Division of Bioinformatics, Walter and Eliza Hall Institute of Medical Research, Parkville, Victoria, Australia; and [5]Department of Medicine, Austin Hospital, Heidelberg, Victoria, Australia

PET offers a noninvasive means to assess neoplasms, in view of its sensitivity and accuracy in staging tumors and potentially in monitoring treatment response. The aim of this study was to evaluate newly diagnosed non–small cell lung cancer (NSCLC) for the presence of hypoxia, as indicated by the uptake of ^{18}F-fluoromisonidazole (^{18}F-FMISO), and to examine the relationship of hypoxia to the uptake of ^{18}F-FDG, microvessel density, and other molecular markers of hypoxia. **Methods:** Twenty-one patients with suspected or biopsy-proven NSCLC were enrolled prospectively in this study. All patients had PET studies with ^{18}F-FMISO and ^{18}F-FDG. Seventeen patients subsequently underwent surgery, with analysis performed for tumor markers of angiogenesis and hypoxia. **Results:** In the 17 patients with resectable NSCLC (13 men, 4 women; age range, 51–77 y), the mean ^{18}F-FMISO uptake in tumor was significantly lower than that of ^{18}F-FDG uptake ($P < 0.0001$) and showed no correlation with ^{18}F-FDG uptake ($r = 0.26$). The mean (95% confidence interval [CI]) ^{18}F-FMISO SUV$_{max}$ (maximum standardized uptake value) was 1.20 [0.95–1.45] compared with the mean [95% CI] ^{18}F-FDG SUV$_{max}$ of 5.99 [4.62–7.35]. The correlation between ^{18}F-FMISO uptake, ^{18}F-FDG uptake, and tumor markers of hypoxia and angiogenesis was poor. A weakly positive correlation between ^{18}F-FMISO and ^{18}F-FDG uptake and Ki67 was found. **Conclusion:** The hypoxic cell fraction of primary NSCLC is consistently low, and there is no significant correlation in NSCLC between hypoxia and glucose metabolism in NSCLC assessed by ^{18}F-FDG. These findings have direct implications in understanding the role of angiogenesis and hypoxia in NSCLC biology.

Key Words: PET; tumor hypoxia; non–small cell lung cancer; immunohistochemistry; vascular endothelial growth factor

J Nucl Med 2006; 47:1921–1926

Tumor hypoxia has been demonstrated to have a significant impact on the biologic behavior of many malignancies, including non–small cell lung cancer (NSCLC), with more hypoxic tumors generally having a more aggressive phenotype and worse prognosis (1–3). It is postulated that one of the mechanisms hypoxia contributes to reduced tumor response to both chemotherapy and radiotherapy is by decreasing the availability of oxygen free radicals, which are necessary to induce sufficient DNA damage to cause cell death (4,5).

The gold standard for determining the degree of tumor hypoxia is, at present, direct measurement of tissue oxygen tension with a probe inserted directly into the tissue of interest, often at the time of surgery (6). This technique has disadvantages, as it is invasive, is subject to potential sampling error, and cannot be applied to tissue that is not easily accessible.

^{18}F-Fluoromisonidazole (^{18}F-FMISO) PET is a recognized noninvasive method of quantifying tumor hypoxia in several solid tumors, including glioma, head and neck cancers, NSCLC, and, to a lesser extent, renal carcinomas (6–9). The application of ^{18}F-FMISO for assessment of the hypoxic fraction in NSCLC is yet to be completely defined. To date, several small studies have evaluated the utility of ^{18}F-FMISO in NSCLC and have focused primarily on predicting response to radiotherapy (9–11). The results have been conflicting, with some evidence to suggest that the outcome after radiotherapy may possibly be predicted on the basis of the kinetic behavior of ^{18}F-FMISO in NSCLC before and after radiotherapy (9).

The relationship between ^{18}F-FMISO uptake in NSCLC and several metabolic parameters, including glucose metabolism, has not been established. The ability to detect and quantify hypoxia has immediate clinical relevance in

NSCLC, because the hypoxic fraction of the tumor at the time of diagnosis may have a significant impact on the treatment outcome and ultimate prognosis.

The aim of this study was to evaluate the degree of hypoxia in NSCLC noninvasively using ^{18}F-FMISO PET and to compare these results with ^{18}F-FDG uptake, immunohistochemistry (IHC) markers of glucose metabolism, hypoxia, proliferation, and degree of tumor differentiation.

MATERIALS AND METHODS

Twenty-one patients with suspected or biopsy-proven NSCLC awaiting surgical resection were enrolled prospectively in this study. All patients had ^{18}F-FDG PET scans before surgery, with 3 patients having ^{18}F-FDG PET scans at an external institution. This protocol was approved by the Austin Hospital Ethics Committee.

PET

^{18}F-FDG and ^{18}F-FMISO were synthesized using ^{18}F produced by an in-house 10-MeV cyclotron (Ion Beam Applications S.A.) as described in previous studies (6,12–14). Samples of ^{18}F-FDG and ^{18}F-FMISO underwent quality control assessment before clinical studies. ^{18}F-FDG and ^{18}F-FMISO studies were performed on separate days. ^{18}F-FMISO scanning was conducted 2 h after the administration of 370 MBq of ^{18}F-FMISO to allow for tracer equilibrium. In-house ^{18}F-FDG PET images were acquired after a minimum of 6 h of fasting, in 2-dimensional mode, and with measured attenuation corrections. PET images were acquired on an ECAT 951/31R PET scanner (CTI PET Systems), an Allegro scanner (Philips), or a Gemini scanner (Philips). The high-sensitivity, 3-dimensional (3D) acquisition mode was used for the ^{18}F-FMISO studies. Measured attenuation correction was performed with the 3D PET datasets reconstructed using a 3D row-action maximum likelihood algorithm (RAMLA). The 3 external ^{18}F-FDG PET scans were performed at an external institution on a Siemens Biograph PET/CT bismuth germanium oxide (BGO) scanner (CTI PET Systems). Calibration with a PET phantom was performed to enable accurate comparison between the 3 external ^{18}F-FDG PET scans and in-house ^{18}F-FDG/^{18}F-FMISO PET scans performed at the Austin Hospital. The PET phantom used was a uniform 6-L cylinder filled with a [68]Ge-gel source of activity (120 MBq). The cylinder was scanned for 20 min in the Gemini PET/CT and the Biograph/BGO scanner. The purpose of the exercise was to determine what DICOM (digital imaging and communication in medicine) fields were used in the Siemens files to produce a standardized uptake value (SUV) image. After determination of these fields, in-house software was modified to report the Siemens PET scans in SUV units for comparison with Gemini SUV units.

PET Data Analysis

Reconstructed PET images were qualitatively analyzed by 2 experienced PET nuclear medicine physicians. Access to the patient's clinical history and corresponding CT scans was available for correlation. The ^{18}F-FMISO and ^{18}F-FDG uptake within the reference lesion relative to comparable normal tissue (contralateral normal lung) was analyzed.

CT Scans

CT scans acquired on an 8-slice Light Speed series CT scanner (GE Healthcare) were obtained on all patients as part of routine surgical work-up. These scans were analyzed to localize the tumor for PET, assess its size, and look for areas of reduced contrast enhancement suggestive of necrosis. After reconstruction of images, the CT scans were used to guide drawing of regions of interest (ROIs) for analysis of each of the PET planes containing tumor.

ROI Analysis

ROI analysis was performed on each subject's original ^{18}F-FDG PET and ^{18}F-FMISO PET data aligned with their CT data. This was achieved by registration of ^{18}F-FDG, ^{18}F-FMISO, and CT images using the Syntegra/Phillips mutual information co-registration algorithm. For each transaxial slice, a ROI was drawn over the contralateral lung and the mean and SD of voxel activity in the ROI were calculated. The SUV_{max} was defined as the highest voxel value within the operator-defined ROI.

Histopathology and Tumor Markers of Hypoxia, Proliferation, and Angiogenesis

The final outcome for the presence of disease was based on histopathology obtained by biopsy or surgical resection, within 2 wk of undergoing the imaging studies. Formalin-fixed, paraffin-embedded tumor tissue from each patient in the study was immunostained by the labeled avidin-biotin method. Negative controls for the immunostaining procedure were prepared by omission of the primary antibody or by using an IgG-matched control antibody. The intensity of staining was described as negative (−), weak (+), moderate (++), and strong (+++).

Positive expression of the markers glucose transporter protein type 1 (GLUT1), nuclear antigen Ki67 (Immunotech), hypoxia-inducible factor 1α (HIF-1α), vascular endothelial growth factor (VEGF), and VEGF receptor (VEGF-R1) (all from Santa Cruz Biotechnology, unless stated otherwise) was determined as follows: Tumor sections were observed in high-power (×400) fields with the aid of a graticule providing an area of 250 μm^2 per field. The number of fields observed was dependent on the amount of viable tissue available, and fields were matched for each marker. The number of tumor cells stained divided by the total number of tumor cells was expressed as a percentage.

Microvessel density (MVD) was determined in the same high-power fields for each patient using staining specific for endothelial cells with Von Willebrand factor (VWF; Dako) to identify individual blood vessels. Vascular structure with visible lumens was considered a single countable microvessel. For statistical comparison with other tumor markers, the raw values of vessels per field were used.

Statistical Methods

The data was analyzed using R v2.0.1 (http://www.r-project.org/). Only data from patients with successfully resected NSCLC was included. As the IHC measurements were expressed as proportions, the arcsine transformation was applied. QQ plots of the transformed data showed it to be reasonably normal, although heavy tails were evident in some cases. Univariate analysis was performed using parametric methods. No correction for multiple testing was performed. The Spearman rank correlation was used to determine the correlation between the grade of tumor and the intrapatient mean of the markers and also to examine correlation between markers.

IHC measurements from the 5 patients with the highest ^{18}F-FMISO SUV_{max} were compared with the remaining 12 patients to evaluate if any significant differences in IHC markers of hypoxia or proliferation were present between the 2 groups. t tests were used to test for difference between the transformed IHC measurements across the 2 groups. ANOVA was used to test individually for differences in PET and IHC measurements across tumor grade and type.

RESULTS

Patients

Twenty-one patients with suspected or biopsy-proven NSCLC were enrolled in the study. Four of the 21 patients were unresectable at surgery and no tissue was obtained. Seventeen patients underwent surgical resection and had histology available for statistical analysis (13 men, 4 women; mean age, 67 y; age range, 51−77 y) (Table 1).

Relationship Between ^{18}F-FMISO and ^{18}F-FDG Uptake in Tumor

^{18}F-FMISO uptake in tumor was low and significantly less than ^{18}F-FDG uptake ($P < 0.0001$) (Fig. 1). ^{18}F-FMISO SUV$_{max}$ ranged from 0.40 to 2.14. ^{18}F-FDG SUV$_{max}$ ranged from 2.16 to 10.46. The mean (95% confidence interval [CI]) ^{18}F-FMISO SUV$_{max}$ was 1.20 [0.95−1.45] compared with the mean [95% CI] ^{18}F-FDG SUV$_{max}$ of 5.99 [4.62−7.35]. No correlation was found between tumor ^{18}F-FMISO SUV$_{max}$ and ^{18}F-FDG SUV$_{max}$ ($r = 0.26$) or between increasing ^{18}F-FMISO tumor-to-background ratio and ^{18}F-FDG SUV$_{max}$ ($r = 0.41$). In the 5 patients with the highest ^{18}F-FMISO uptake (patients 6, 10, 14, 15, and 17), where uptake was sufficient for meaningful qualitative visual comparison with ^{18}F-FDG uptake, the pattern of ^{18}F-FMISO uptake was more heterogeneous than that of ^{18}F-FDG uptake and showed prominence in the periphery of the tumor mass (Fig. 2).

Relationship Between ^{18}F-FMISO/^{18}F-FDG Uptake and Tumor Markers of Hypoxia, Proliferation, and Angiogenesis

Correlation between ^{18}F-FMISO and ^{18}F-FDG uptake with tumor markers of hypoxia and angiogenesis was poor. No correlation was seen between either ^{18}F-FMISO or ^{18}F-FDG uptake and MVD, HIF-1α, VEGF, VEGF-R1, and GLUT1 expression. A weakly positive correlation between both ^{18}F -FMISO ($r = 0.64$) and ^{18}F-FDG uptake ($r = 0.75$) and the proliferative marker Ki67 was demonstrated in peripheral tumor, with no correlation seen in central tumor. There was no correlation between ^{18}F-FMISO SUV$_{max}$ and the degree of NSCLC differentiation on the basis of ANOVA analysis ($P = 0.993$). Similarly, there was no correlation between ^{18}F-FDG SUV$_{max}$ and the degree of NSCLC differentiation on the basis of ANOVA analysis ($P = 0.146$). The 5 patients with the highest ^{18}F-FMISO uptake (patients 6, 10, 14, 15, and 17) were evaluated to determine if they had any IHC characteristics that set them apart from the other 12 patients. Only Ki67 expression was statistically different between these 5 patients and the other 12 patients (60% vs. 24%, $P = 0.00044$).

Tumor Differentiation and Markers of Hypoxia, Proliferation, and Angiogenesis

Staining was relatively homogeneous within tumor for all markers studied except for GLUT1, where patchy staining was observed generally surrounding areas of necrosis in

TABLE 1
Patient Characteristics and Imaging Data

| Patient no.	Age (y)	Sex	Tumor differentiation*	Stage at surgery†	Histology‡	^{18}F-FDG SUV$_{max}$ (T)§	^{18}F-FMISO SUV$_{max}$ (T)‖	^{18}F-FMISO T/N¶
1	72	F	Moderate	I (T1 N0 M0)	Adeno Ca	3.50	1.0	1.67
2	68	M	Moderate	I (T1 N0 M0)	Adeno Ca	2.80	1.3	1.18
3	51	M	Moderate	II (T1 N1 M0)	Adeno/SCC	5.90	1.0	2.00
4	69	M	Poor	I (T1 N0 M0)	Adeno Ca	4.50	1.25	1.98
5	66	M	Poor	I (T1 N0 M0)	Adeno Ca	4.15	1.10	2.20
6	59	M	Poor	I (T1 N0 M0)	Adeno Ca	9.38	1.70	4.25
7	69	M	Poor	I (T1 N0 M0)	Adeno Ca	6.40	0.80	1.60
8	77	M	Moderate	I (T1 N0 M0)	Adeno/SCC	2.91	0.91	3.25
9	71	M	Moderate	I (T1 N0 M0)	Adeno Ca	7.20	0.86	2.32
10	73	M	Moderate	II (T1 N1 M0)	SCC	8.30	1.74	4.46
11	66	M	Poor	I (T1 N0 M0)	Adeno Ca	2.63	0.75	4.41
12	70	M	Moderate	I (T1 N0 M0)	SCC	8.72	0.59	5.36
13	69	M	Moderate	I (T1 N0 M0)	SCC	6.54	0.40	2.86
14	58	F	Well	I (T1 N0 M0)	Adeno Ca	2.16	1.61	5.75
15	63	F	Moderate	I (T1 N0 M0)	Adeno Ca	8.53	2.14	9.73
16	75	F	Poor	I (T1 N0 M0)	Adeno Ca	10.46	1.46	5.21
17	63	M	Moderate	I (T1 N0 M0)	Adeno Ca	7.71	1.82	5.06

*Well, moderate, or poorly differentiated tumor.
†Based on American Joint Committee on Cancer NSCLC staging system (2002).
‡Adeno Ca = adenocarcinoma; Adeno/SCC = mixed adenocarcinoma/squamous carcinoma; SCC = squamous cell carcinoma.
§^{18}F-FDG SUV$_{max}$ in tumor.
‖^{18}F-FMISO SUV$_{max}$ in tumor.
¶^{18}F-FMISO SUV$_{max}$ in tumor/^{18}F-FMISO SUV$_{max}$ uptake in normal lung.
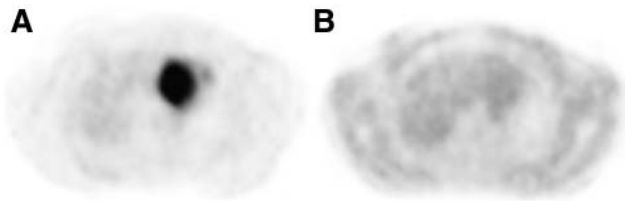
FIGURE 1. ^{18}F-FDG and ^{18}F-FMISO PET scans in patient 12. (A) Intense uniform ^{18}F-FDG uptake in tumor. (B) ^{18}F-FMISO uptake in tumor similar to that of blood pool.

some tumors. The amount of tumor necrosis increased with decreasing tumor differentiation. Poorly differentiated tumors contained up to 25%−50% cell necrosis. Membrane and cytoplasmic staining patterns were observed for GLUT1, whereas VEGF, VEGF-R1, and HIF-1α were predominantly expressed in the cytoplasm with some nuclear staining. Ki67 exhibited nuclear staining (Fig. 3). A trend of decreasing MVD was seen with decreasing tumor differentiation.

Relationship Between HIF-1α Expression and Markers of Hypoxia/Proliferation

HIF-1α expression was detected in all tumors. HIF-1α nuclear expression was divided into 2 groups on the basis of median HIF-1α expression, which permitted a 2-factor statistical analysis with other markers. No significant differences were found in the levels of expression of GLUT1, Ki67, VEGF, VEGF-R1, and MVD between regions of higher HIF-1α nuclear expression and regions of lower HIF-1α nuclear expression.

Relationship Between MVD and Markers of Hypoxia/Proliferation

MVD measured by VWF staining was generally low, with normal lung parenchyma demonstrating significantly higher vascularity ($P = 0.004$). The mean MVD [95% CI] in tumor was 1.56 [1.00−2.12] vessels per high-power field (×400) compared with the mean MVD [95% CI] of 3.96 [2.87−5.05] in normal lung. MVD as measured by VWF was divided into 2 groups on the basis of median vessel density, which permitted a 2-factor statistical analysis with other markers. GLUT1 ($P = 0.001$) and Ki67 ($P = 0.036$) expression was significantly greater in the lower MVD group.
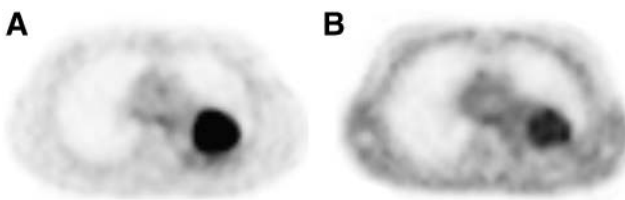
FIGURE 2. ^{18}F-FDG and ^{18}F-FMISO PET scans in patient 15. (A) Intense uniform ^{18}F-FDG uptake in tumor. (B) Heterogeneous mildly increased ^{18}F-FMISO uptake with more prominent uptake in periphery of tumor.

DISCUSSION

Lung cancer is one of the leading causes of cancer death in the United States and Australia. Most (~80%) lung cancers are NSCLC, and at least 65% of patients present with incurable stage IIIB or stage IV disease (*15*). The overall 5-y survival rate for this subset of patients is typically 6−9 mo after standard platinum-based therapy (*15*). Clearly, more effective treatment regimens are required to combat this increasingly prevalent condition.

Tumor hypoxia has been identified as a major independent prognostic factor influencing response to therapy and overall survival in many malignancies, including NSCLC (*16,17*). Many different techniques have been developed to evaluate the oxygenation status of tumors, but none has entered widespread clinical use (*8*), with direct measurement of the partial pressure of oxygen (Po_2) by an oxygen microelectrode still considered the gold standard (*18,19*). Intratumoural hypoxia cannot be predicted by size, grade, or histology of the tumor (*20,21*).

PET studies with hypoxia-sensitive radiotracers such as ^{18}F-FMISO allow quantification of tumor hypoxia noninvasively and may have a significant role in the management of NSCLC because of their potential to provide prognostic information and guide or monitor treatment response on a regular basis.

The results of our study have shown that ^{18}F-FMISO uptake is not correlated with, and is considerably lower than, ^{18}F-FDG uptake in NSCLC. The pattern of ^{18}F-FMISO uptake in tumor is also different than that of ^{18}F-FDG, tending to be more heterogeneous and, where ^{18}F-FMISO uptake is prominent, more clearly seen in the periphery of tumor masses. These findings are novel and support the observation that regional hypoxia does not correlate with glucose metabolism in NSCLC.

^{18}F-FMISO uptake is increased only when tissue hypoxia of <10 mm Hg is present (*22,23*). The low overall uptake of ^{18}F-FMISO seen in our cohort of patients suggests that NSCLC may not be as hypoxic as other tumors, such as head and neck cancers, despite having similar clinical characteristics, such as resistance to therapy. It is possible that the unique structure of lung parenchyma, including its dual blood supply and abundant oxygen-containing air spaces, may play a role in NSCLC being less hypoxic than other tumor types.

A review of the literature supports the hypothesis that NSCLC is a less-hypoxic tumor. In a recently published study by Le et al. (*2*), Po_2 was measured invasively with an Eppendorf polarographic electrode in 20 patients with NSCLC. The median Po_2 was 16.6 mm Hg (range, 0.7–46 mm Hg), which is above the threshold for ^{18}F-FMISO uptake. The addition to our study of several patients with invasive probe measurements of NSCLC tumor oxygenation is planned at our institution to confirm these findings.

Another possible explanation or contributing factor to the low degree of overall ^{18}F-FMISO uptake in our cohort of patients is the presence of tumor necrosis. Metabolic
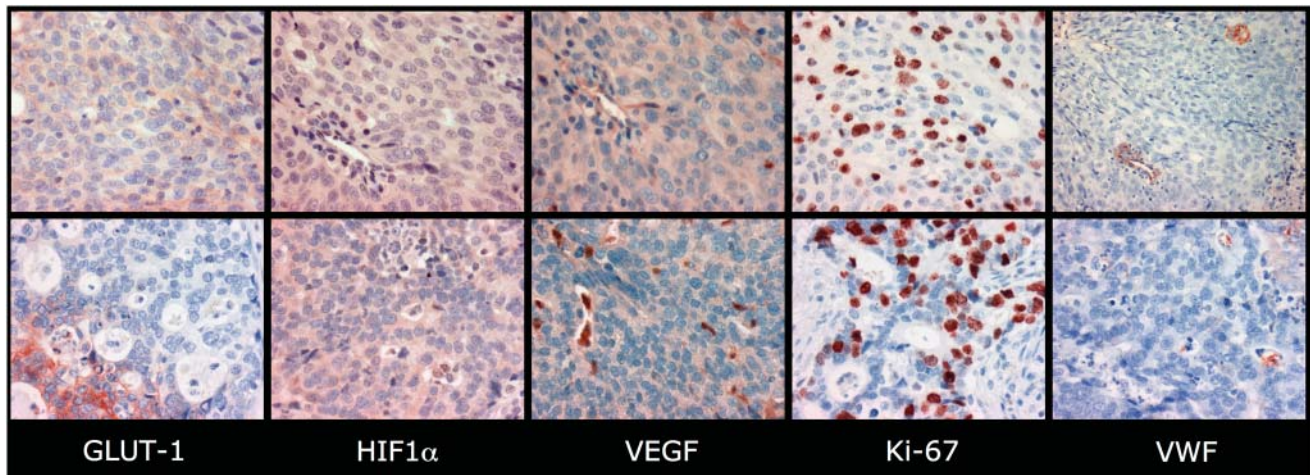
FIGURE 3. IHC of tumor biopsies from 2 representative patients. (Top row) Moderately differentiated squamous cell carcinoma (patient 12) with high ^{18}F-FDG uptake and minimal ^{18}F-FMISO uptake on PET studies. (Bottom row) Moderately differentiated adenocarcinoma (patient 15) in which expression of all tumor markers was similar despite higher ^{18}F-FMISO uptake on PET studies. (GLUT1, HIF-1α, VEGF, and Ki67, ×400; VWF, ×200)

trapping of ^{18}F-FMISO requires an intact intracellular electron transport system—hence, no accumulation occurs in necrotic cells (*24,25*). Histopathology revealed significant areas of tumor necrosis, particularly in less-differentiated tumors. This is likely to have a significant impact on reducing overall ^{18}F-FMISO uptake. However, the uniform uptake of ^{18}F-FDG in tumor masses in most patients does make the impact of necrosis on ^{18}F-FMISO uptake less likely.

A combination of factors influencing ^{18}F-FMISO uptake, including those discussed here, possibly explains the lack of correlation between ^{18}F-FMISO uptake and tumor markers of hypoxia and angiogenesis.

HIF-1α nuclear expression in tumor was variable, with levels comparable with other HIF-1α studies in NSCLC (*1,26–28*); however, unusually high expression of HIF-1α was seen in cytoplasm (90%−100% in most cases). This finding suggests that an artifact or hypoxia may have been introduced during the collection process, causing artificially elevated cytoplasmic HIF-1α levels. The HIF-1α assay is difficult to perform and the opportunity for HIF-1α expression in the interval between resection and imbedding remains because cells become anoxic during this time. Because of these possible spurious results, only HIF-1α nuclear expression was analyzed and compared with imaging results and other markers of hypoxia and proliferation.

Although overall NSCLC MVD was low compared with that of normal lung parenchyma, tumors with the lowest MVD demonstrated significantly higher GLUT1 and Ki67 expression, suggestive of a more aggressive phenotype and a worse prognosis. Volm et al. reported similar findings in which NSCLC tumors with the lowest MVD were more resistant to doxorubicin-based chemotherapy and had a worse prognosis (*29*).

Despite VEGF expression being a major factor implicated in angiogenesis in NSCLC, evidence for VEGF expression correlating with hypoxia is conflicting. Several studies suggest a relationship between hypoxia, HIF-1α, and VEGF expression (*27,30*), whereas other studies have not demonstrated any significant relationship (*1*). In our study, VEGF and VEGF-R1 expression in peripheral and central tumor was uniformly high (100% in most cases) across all tumor types—regardless of the degree of tumor differentiation—and appeared independent of any markers of hypoxia or proliferation.

One of the main aims of functional imaging of tumoral hypoxia is to localize subpopulations that are more likely to be resistant to radiotherapy and chemotherapy, which would enable the tailoring of treatment, such as deposition of higher radiation doses in hypoxic areas, while minimizing doses to well-oxygenated areas. Similarly, the use of chemotherapeutic agents (e.g., tirapazamine) that target hypoxic tissues may be chosen in tumors in which significant hypoxia is present. The use of agents such as efaproxiral (RSR-13), which reverse tumor hypoxia, could also be considered in combination with chemotherapy and radiotherapy in tumors deemed more hypoxic on functional imaging, which may translate into improved treatment outcome (*31*). Ultimately, imaging hypoxia with techniques such as ^{18}F-FMISO PET may have a role not only in directing patients toward targeted hypoxic therapies but also in monitoring response to such therapies.

CONCLUSION

The hypoxic cell fraction of primary NSCLC measured by ^{18}F-FMISO is consistently low, and there is no significant correlation in NSCLC between hypoxia and glucose metabolism in NSCLC assessed by ^{18}F-FDG. These findings have direct implications in understanding the role of angiogenesis and hypoxia in NSCLC biology.

REFERENCES

1. Kim SJ, Rabbani ZN, Dewhirst MW, et al. Expression of HIF-1alpha, CA IX, VEGF, and MMP-9 in surgically resected non-small cell lung cancer. *Lung Cancer.* 2005;49:325–335.
2. Le QT, Chen E, Salim A, et al. An evaluation of tumor oxygenation and gene expression in patients with early stage non-small cell lung cancers. *Clin Cancer Res.* 2006;12:1507–1514.
3. Koukourakis MI, Giatromanolaki A, Sivridis E, et al. Lactate dehydrogenase-5 (LDH-5) overexpression in non-small-cell lung cancer tissues is linked to tumour hypoxia, angiogenic factor production and poor prognosis. *Br J Cancer.* 2003;89:877–885.
4. Gray LH, Conger AD, Ebert M, Hornsey S, Scott OC. The concentration of oxygen dissolved in tissues at the time of irradiation as a factor in radiotherapy. *Br J Radiol.* 1953;26:638–648.
5. Lewis JS, Welch MJ. PET imaging of hypoxia. *Q J Nucl Med.* 2001;45:183–188.
6. Cher LM, Murone C, Lawrentschuk N, et al. Correlation of hypoxic cell fraction and angiogenesis with glucose metabolic rate in gliomas using ^{18}F-fluoromisonidazole, ^{18}F-FDG PET, and immunohistochemical studies. *J Nucl Med.* 2006;47:410–418.
7. Hicks RJ, Rischin D, Fisher R, Binns D, Scott AM, Peters LJ. Utility of FMISO PET in advanced head and neck cancer treated with chemoradiation incorporating a hypoxia-targeting chemotherapy agent. *Eur J Nucl Med Mol Imaging.* 2005;32:1384–1391.
8. Lawrentschuk N, Poon AM, Foo SS, et al. Assessing regional hypoxia in human renal tumours using ^{18}F-fluoromisonidazole positron emission tomography. *BJU Int.* 2005;96:540–546.
9. Eschmann SM, Paulsen F, Reimold M, et al. Prognostic impact of hypoxia imaging with ^{18}F-misonidazole PET in non-small cell lung cancer and head and neck cancer before radiotherapy. *J Nucl Med.* 2005;46:253–260.
10. Koh WJ, Bergman KS, Rasey JS, et al. Evaluation of oxygenation status during fractionated radiotherapy in human nonsmall cell lung cancers using [F-18] fluoromisonidazole positron emission tomography. *Int J Radiat Oncol Biol Phys.* 1995;33:391–398.
11. Gagel B, Reinartz P, Demirel C, et al. [18F] fluoromisonidazole and [18F] fluorodeoxyglucose positron emission tomography in response evaluation after chemo-/radiotherapy of non-small-cell lung cancer: a feasibility study. *BMC Cancer.* 2006;6:51.
12. Read SJ, Hirano T, Abbott DF, et al. The fate of hypoxic tissue on ^{18}F-fluoromisonidazole positron emission tomography after ischemic stroke. *Ann Neurol.* 2000;48:228–235.
13. Read SJ, Hirano T, Abbott DF, et al. Identifying hypoxic tissue after acute ischemic stroke using PET and ^{18}F-fluoromisonidazole. *Neurology.* 1998;51:1617–1621.
14. Johns Putra L, Lawrentschuk N, Ballok Z, et al. ^{18}F-Fluorodeoxyglucose positron emission tomography in evaluation of germ cell tumor after chemotherapy. *Urology.* 2004;64:1202–1207.
15. Spiro SG, Silvestri GA. The treatment of advanced non-small cell lung cancer. *Curr Opin Pulm Med.* 2005;11:287–291.
16. Dachs GU, Tozer GM. Hypoxia modulated gene expression: angiogenesis, metastasis and therapeutic exploitation. *Eur J Cancer.* 2000;36(13):1649–1660.
17. Tsang RW, Fyles AW, Milosevic M, et al. Interrelationship of proliferation and hypoxia in carcinoma of the cervix. *Int J Radiat Oncol Biol Phys.* 2000;46:95–99.
18. Nordsmark M, Bentzen SM, Overgaard J. Measurement of human tumour oxygenation status by a polarographic needle electrode: an analysis of inter- and intratumour heterogeneity. *Acta Oncol.* 1994;33:383–389.
19. Foo SS, Abbott DF, Lawrentschuk N, Scott AM. Functional imaging of intratumoral hypoxia. *Mol Imaging Biol.* 2004;6:291–305.
20. Hockel M, Vaupel P. Biological consequences of tumor hypoxia. *Semin Oncol.* 2001; 28(2 suppl 8)36–41.
21. Hockel M, Schlenger K, Aral B, Mitze M, Schaffer U, Vaupel P. Association between tumor hypoxia and malignant progression in advanced cancer of the uterine cervix. *Cancer Res.* 1996;56:4509–4515.
22. Koch CJ, Evans SM. Non-invasive PET and SPECT imaging of tissue hypoxia using isotopically labeled 2-nitroimidazoles. *Adv Exp Med Biol.* 2003;510:285–292.
23. Rasey JS, Nelson NJ, Chin L, Evans ML, Grunbaum Z. Characteristics of the binding of labeled fluoromisonidazole in cells in vitro. *Radiat Res.* 1990;122:301–308.
24. Rasey JS, Grunbaum Z, Magee S, et al. Characterization of radiolabeled fluoromisonidazole as a probe for hypoxic cells. *Radiat Res.* 1987;111:292–304.
25. Graham MM, Peterson LM, Link JM, et al. Fluorine-18-fluoromisonidazole radiation dosimetry in imaging studies. *J Nucl Med.* 1997;38:1631–1636.
26. Swinson DE, Jones JL, Cox G, Richardson D, Harris AL, O'Byrne KJ. Hypoxia-inducible factor-1 alpha in non small cell lung cancer: relation to growth factor, protease and apoptosis pathways. *Int J Cancer.* 2004;111:43–50.
27. Giatromanolaki A, Koukourakis MI, Sivridis E, et al. Relation of hypoxia inducible factor 1 alpha and 2 alpha in operable non-small cell lung cancer to angiogenic/molecular profile of tumours and survival. *Br J Cancer.* 2001;85:881–890.
28. Volm M, Koomagi R. Hypoxia-inducible factor (HIF-1) and its relationship to apoptosis and proliferation in lung cancer. *Anticancer Res.* 2000;20:1527–1533.
29. Volm M, Koomagi R, Mattern J. Interrelationships between microvessel density, expression of VEGF and resistance to doxorubicin of non-small lung cell carcinoma. *Anticancer Res.* 1996;16:213–217.
30. Zhang H, Zhang Z, Xu Y, et al. The expression of hypoxia inducible factor 1-alpha in lung cancer and its correlation with P53 and VEGF. *J Huazhong Univ Sci Technolog Med Sci.* 2004;24:124–127.
31. Choy H, Nabid A, Stea B, et al. Phase II multicenter study of induction chemotherapy followed by concurrent efaproxiral (RSR13) and thoracic radiotherapy for patients with locally advanced non-small-cell lung cancer. *J Clin Oncol.* 2005;23:5918–5928.